

# A POMT2 missense substitution contributes to hypoxia adaptation in hibernating mammals

Jinjin Zhang <sup>1,†</sup>, Xiuping Zhang <sup>1,†</sup>, Ningyawen Liu <sup>1,2</sup>, Jiang Hu <sup>3</sup>, Michael Hiller <sup>4,5,6</sup>,  
Virag Sharma <sup>7</sup>, Fengming Han <sup>8</sup>, He Dai <sup>9</sup>, Xiaolong Tu <sup>1</sup>, David N. Cooper <sup>10</sup>,  
Dong-Dong Wu <sup>1,11</sup>, Lin Zeng <sup>1,12,\*</sup>

<sup>1</sup>State Key Laboratory of Genetic Evolution & Animal Models, Kunming Institute of Zoology, Chinese Academy of Sciences, Kunming, Yunnan 650223, China

<sup>2</sup>Kunming College of Life Science, University of the Chinese Academy of Sciences, Kunming 650204, China

<sup>3</sup>GrandOmics Biosciences, Beijing 102206, China

<sup>4</sup>LOEWE Centre for Translational Biodiversity Genomics, Senckenberganlage 25, Frankfurt 60325, Germany

<sup>5</sup>Senckenberg Research Institute, Senckenberganlage 25, Frankfurt 60325, Germany

<sup>6</sup>Institute of Cell Biology and Neuroscience, Faculty of Biosciences, Goethe University Frankfurt, Max-von-Laue-Str. 9, Frankfurt 60438, Germany

<sup>7</sup>Max Planck Institute of Molecular Cell Biology and Genetics, 01307 Dresden, Germany

<sup>8</sup>Shandong BellaGen Biotechnology Co., Ltd., Shandong 250300, China

<sup>9</sup>Biomarker Technologies Corporation, Beijing 101301, China

<sup>10</sup>Institute of Medical Genetics, School of Medicine, Cardiff University, Cardiff, UK

<sup>11</sup>National Resource Center for Non-Human Primates, Kunming Primate Research Center, and National Research Facility for Phenotypic & Genetic Analysis of Model Animals, Primate Facility, Kunming Institute of Zoology, Chinese Academy of Sciences, Kunming, Yunnan 650107, China

<sup>12</sup>Yunnan Key Laboratory of Biodiversity Information, Kunming, Yunnan 650223, China

<sup>†</sup>These authors contributed equally to this work.

\*Corresponding author: E-mail: [zenglin@mail.kiz.ac.cn](mailto:zenglin@mail.kiz.ac.cn).

Associate editor: Xuming Zhou

## Abstract

Hibernation is an adaptive survival strategy used by animals to cope with extreme environmental conditions. Although this physiological process involves complex metabolic changes, its underlying biological mechanisms remain largely unknown. Through comparative genomic analysis of six hibernating species across five orders, we identified an ancient amino acid substitution in POMT2 (R708Q), exhibiting signals of both convergent and positive selection in hibernating mammals. Phylogenetic analysis using HeIST indicated hemiplasy as a possible explanation, though given mammalian divergence times and the broader evidence for convergence, this is best considered an alternative rather than the primary interpretation. Functional studies using transgenic mice demonstrated the contribution of this mutation to hypoxia adaptation. Notably, despite the absence of this mutation in Rodentia hibernators, we included *Graphiurus kelleni* as a positive control in physiological studies of transgenic mice carrying POMT2 (R708Q), given its remarkable hypoxia adaptation during hibernation. Our findings not only provide novel insights into the genetic basis of hypoxic adaptation in hibernating mammals but also suggest incomplete lineage sorting (hemiplasy) as a plausible evolutionary mechanism for this important adaptive trait.

**Keywords** hibernation, torpor, hypoxia, adaptation, *POMT2*, *Graphiurus kelleni*, dormouse

## Introduction

Hibernation, a physiological state characterized by minimal activity, metabolic suppression, and hypothermia, occurs across diverse mammalian clades including Primates, Chiroptera, Insectivora, Rodentia, and Carnivora. This extreme physiological adaptation serves as an evolutionary strategy to conserve energy and overcome winter challenges such as food scarcity, extreme

temperatures, and predator avoidance, thereby significantly enhancing survival prospects (Geiser 2013). Remarkably, hibernating mammals can tolerate core body temperatures as low as 5 °C without sustaining tissue damage, a physiological feat that would prove fatal to non-hibernating species. Current research has primarily focused on elucidating the mechanisms underlying this exceptional cold tolerance. For instance, studies on 13-lined ground squirrels revealed that induced pluripotent stem cells

**Received:** December 3, 2024. **Revised:** November 6, 2025. **Accepted:** December 2, 2025

© The Author(s) 2026. Published by Oxford University Press on behalf of Society for Molecular Biology and Evolution.

This is an Open Access article distributed under the terms of the Creative Commons Attribution-NonCommercial License (<https://creativecommons.org/licenses/by-nc/4.0/>), which permits non-commercial re-use, distribution, and reproduction in any medium, provided the original work is properly cited. For commercial re-use, please contact [reprints@oup.com](mailto:reprints@oup.com) for reprints and translation rights for reprints. All other permissions can be obtained through our RightsLink service via the Permissions link on the article page on our site—for further information please contact [journals.permissions@oup.com](mailto:journals.permissions@oup.com).

maintain inherent cold-resistant properties, including microtubule stability. Furthermore, [Ou et al. \(2018\)](#) identified critical cellular pathways connecting mitochondria-initiated oxidative stress and lysosomal dysfunction with cold-induced microtubule instability ([Ou et al. 2018](#)). Transcriptomic analyses of Himalayan marmots during hibernation demonstrated significant alterations in hepatic fatty acid metabolism genes, along with modulation of complement and coagulation cascades and stem cell pluripotency pathways in brain tissue ([Bai et al. 2019](#)). [Matos-Cruz et al. \(2017\)](#) discovered specialized modifications in the core trans-membrane domain of the cold-sensing channel TRPM8 in ground squirrels and hamsters ([Matos-Cruz et al. 2017](#)). Proteomic studies of hibernating brown bears revealed that HSP47 down-regulation confers thrombo protection, a mechanism conserved in mice and human spinal cord injury patients ([Thienel et al. 2023](#)). Additionally, [Yang et al. \(2023\)](#) advanced our understanding of cardio-protection in hibernating Daurian ground squirrels through integrated transcriptomic and metabolomic approaches ([Yang et al. 2023](#)).

As mentioned above, hibernating animals exhibit distinct physiological characteristics during hibernation, including decreased body temperature, slowed metabolism, and reduced oxygen consumption. Previous studies have elucidated various molecular mechanisms underlying hibernation across different species. Oxygen plays a fundamental role in sustaining intracellular bioenergetics and is consumed by numerous biochemical reactions. Consequently, hypoxia represents a major physiological stressor that typically disrupts normal life processes in aerobic organisms and is a hallmark of pathological conditions in many diseases, including cancer ([Lee et al. 2020](#)). We hypothesized that hibernating animals possess enhanced adaptation and tolerance to low-oxygen environments during hibernation or torpor, allowing them to endure prolonged hypoxic conditions more effectively than non-hibernating species such as mice. Prior research has identified differences in hypoxia-related gene expression during torpor ([Biggar et al. 2015](#)). Given the characteristic reduction in oxygen consumption during hibernation, this study investigates the phenotypic and molecular mechanisms of hypoxia adaptation in hibernating animals. To further explore the molecular basis of adaptive evolution in hibernation, we employed comparative genomics to analyze convergent evolution across five well-established hibernating lineages (Rodentia, Primates, Carnivora, Chiroptera, and Insectivora). Through comprehensive bioinformatics analyses and functional assessment of candidate convergent sites, we identified a specific amino acid substitution in *POMT2* with a high probability of association with hypoxia adaptation mechanisms. Subsequent functional validation using transgenic mice carrying this mutation confirmed our findings.

In this study, we newly assembled the genomes of two hibernating species: *Graphiurus kelleni* (hereafter referred to as the dormouse/dormice) and *Nyctereutes procyonoides* (raccoon dog). Beyond incorporating these genomes into comparative genomic analyses, we present the first evidence that *G. kelleni* exhibits hibernation behavior. Based on our observations, this species can enter torpor or prolonged torpor (i.e. hibernation) under cold ambient temperatures, irrespective of seasonal cues, indicating facultative hibernation, a stress-induced response triggered by environmental challenges. It played a pivotal role in our physiological investigations of hibernation and hypoxia

adaptation, notably serving as a positive control in functional studies of transgenic mice carrying the *POMT2* (R708Q) mutation. Although this species lacks the specific convergent mutation of interest in our study, it represents a physiologically convergent model for hibernation-related hypoxia adaptation.

## Results

### Comparative genomics analysis identified an evolutionary site of amino acid substitution in *POMT2* in hibernating mammals

To investigate the molecular basis of hibernation evolution across mammalian species, we performed de novo genome sequencing and assembly of two hibernating mammals: Kellen's dormouse (*G. kelleni*) and raccoon dog (*N. procyonoides*) using long-read sequencing technology ([Figures S1 to S4](#) and [Tables S1 to S5](#)). Following assembly refinement with short-read polishing, we achieved high-quality genome assemblies with contig N50 values of 26.6 Mb and 51.5 Mb for the dormouse and raccoon dog, respectively. BUSCO v3.0.1 ([Simão et al. 2015](#)) assessments demonstrated excellent completeness, with 95.2% and 95.6% of core eukaryotic genes identified in the dormouse and raccoon dog assemblies. Using CESAR ([Sharma and Hiller 2019](#)), we annotated 18,415 and 17,544 protein-coding genes in the dormouse and raccoon dog genomes, respectively. Together with genomes from Ensembl (<http://www.ensembl.org/>), the western European hedgehog (*Erinaceus europaeus*), American black bear (*Ursus americanus*), loris (*Nycticebus coucang*), and the great roundleaf bat (*Hipposideros armiger*), we were able to obtain a total of six hibernating mammal genomes. For comparative analysis, we included five non-hibernating representatives from corresponding lineages: mouse (*Mus musculus*), cat (*Felis catus*), Eurasian shrew (*Sorex araneus*), human (*Homo sapiens*), and flying fox (*Pteropus alecto*). The common ancestor, nine-banded armadillo (*Dasypus novemcinctus*) served as the outgroup lineage ([Fig. 1a](#)). From these 12 mammalian genomes, we identified 5,561 high-confidence one-to-one orthologous protein-coding genes for downstream analysis.

Based on the CCS (convergence at conservative sites) method ([Xu et al. 2017](#)), we established a phylogenetic framework comprising six hibernating mammals as the foreground convergent clade, five non-hibernating mammals as background lineages, and the nine-banded armadillo as the outgroup. Convergence is inferred exclusively at conservative sites where either all five non-hibernating species or all six hibernators shared the same character as the outgroup. Additionally, we required that at least four hibernating species (more than half of the six hibernators) share identical derived mutations. Given that convergent amino acid substitutions may arise through positive selection ([Foote et al. 2015](#)) and potentially contribute to hibernation phenotypes, we employed the MEME (mixed effects model of evolution) method in HyPhy to identify codon sites under episodic positive selection in at least four hibernating species. Employing our stringent screening criteria, the CCS method identified 234 convergence sites (representing 234 out of 261,385 conservative

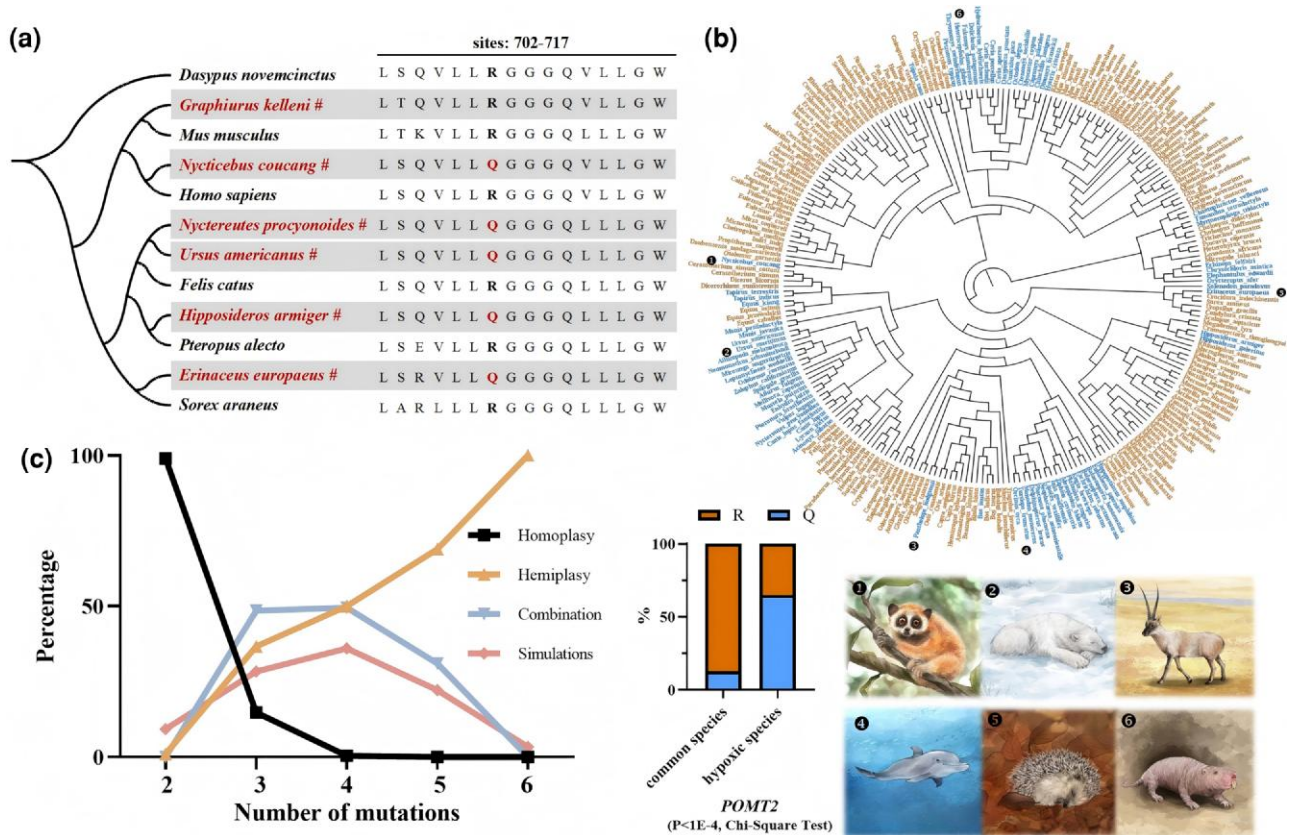


**Figure 1** Comparative genomics analysis. a) Phylogenetic tree of 12 species of mammal used for comparative genomics analysis. Hibernating species are indicated by red color and gray bars. The displayed POMT2 protein segment shows the R708Q amino acid substitution marked in red. b) Phylogenetic tree of 244 mammalian species. Blue denotes 74 species with Q at POMT2 amino acid residue 708 (including 54 hypoxic mammals); species with R residues at this location are shown in orange. The frequency of the 708Q replacement in hypoxic mammals versus in other mammals (65.06% vs. 34.94%,  $\chi^2$  test,  $P < 1E-4$ ). Pictures represent part of the hypoxic species. c) Using the method of HeIST to make statistical inferences about the relative probabilities of hemiplasy and homoplasy which may have led to the POMT2 R708Q substitution based on randomly selected species ( $n = 20$ ) from our phylogenetic tree, and the result showed that hemiplasy was associated with a higher probability of causing the amino acid change.

sites), dispersed across 110 genes. In contrast, MEME identified 149 sites of positive selection (representing 149 out of 4,768,167 sites), distributed among 105 genes. Intersection of these results yielded 10 high-confidence candidate sites for convergent evolution (corresponding genes: *POMT2*, *ZMYND12*, *CABIN1*, *FASTKD2*, *IREB2*, *ZNF462*, *WDR19*, *SLX4*, *DCHS2* and *BRINP2*; Tables S6 to S9). Although these genes have not been previously directly associated with hibernation, their known biological functions suggest plausible connections to hibernation-related traits. For instance, *IREB2* regulates cellular iron homeostasis and may contribute to hypoxia adaptation and oxidative stress resistance during hibernation; *SLX4* maintains genome stability and could protect against cold-induced DNA damage; *FASTKD2* modulates mitochondrial apoptosis and may support mitochondrial function under low metabolic states. Nevertheless, these functional associations remain speculative and require experimental validation.

Given our focus on hypoxia adaptation in hibernating species, we systematically evaluated candidate functional loci by analyzing their prevalence among hypoxic mammals (including aquatic mammals, plateau species, subterranean, diving species) across a broad taxonomic spectrum (covering 244 mammals from the Zoonomia Consortium dataset (Zoonomia Consortium 2020)). Our analysis revealed that the POMT2 708Q variant exhibited

the highest representation among hypoxia-adapted species (65.06%;  $\chi^2$  test,  $P < 1E-4$ ; Fig. 1b; Figure S5 and Table S10). This statistically significant enrichment suggests that this locus has a high probability of association with hypoxia adaptation mechanisms, warranting its selection as the primary candidate for subsequent functional investigations. While our study identified strong signatures of selection at POMT2 R708Q, as well as at the gene level when using BUSTED as a complementary test for gene-wide selection (Table S11), this single-locus approach may not capture polygenic adaptive mechanisms. Future genome-wide association studies in larger hibernator cohorts could reveal additional selected loci.

To elucidate the evolutionary origin of the POMT2 R708Q substitution, we conducted comprehensive phylogenetic analyses across mammalian lineages. Our investigation revealed this substitution's presence extends deep into evolutionary time, traceable to marsupials, with widespread distribution among both hibernating and hypoxic mammals (Fig. 1b; Table S10). The occurrence of the R708Q substitution in some non-hibernating and non-hypoxic mammals suggests this substitution did not emerge through convergent evolution. Rather, we hypothesize the observed phylogenetic incongruence reflects maintenance of an ancestral trans-species polymorphism that persisted following mammalian lineage diversification. To test this

hypothesis, we first applied PCOC analysis (Rey et al. 2018) to evaluate whether this substitution represented a convergent shift coinciding with phenotypic changes. The results demonstrated an exceptionally low posterior probability ( $3.89E-25$ ) for convergent evolution relative to the null model (Figures S6 and S7 and Table S12), effectively excluding convergence as a plausible mechanism. Given that hemiplasy can produce similar phylogenetic patterns to homoplasy, we subsequently employed the HeIST framework (Hibbins et al. 2020) to statistically compare these alternative evolutionary scenarios. Using HeIST's Fitch parsimony approach, we quantified the number of required amino acid substitutions needed to explain the observed trait distribution across phylogenetically informed random datasets (Fig. 1b). We conducted extensive phylogenetic simulations across 1,500 datasets stratified into three size categories (20, 25, and 30 randomly selected species from our phylogenetic tree). Initial analyses revealed that simulations with 25 and 30 species produced an unacceptably low proportion of valid outputs (<50%) containing the focal loci (Figure S8 and Table S13), prompting us to focus subsequent analyses on the more reliable 20-species datasets. Within these optimized simulations, our results demonstrated that hemiplasy showed significantly higher probability than homoplasy of explaining the observed amino acid substitution pattern when three or more independent ancestral substitutions were required to produce the current state (Fig. 1c; Table S14). Nevertheless, we cannot entirely exclude the possibility of multiple independent origins for this substitution across different genetic backgrounds during mammalian evolution, as the R708Q replacement occurs in a CpG-containing codon (CGA to CAA), which represents one of the most pronounced mutational hotspots in mammalian genomes (Azevedo et al. 2015).

## The transgenic mice carrying POMT2 (R708Q) exhibited a hypoxia-adapted phenotype

To investigate the functional significance of the POMT2 R708Q substitution in hypoxia adaptation, we generated homozygous transgenic mice (*M. musculus* carrying POMT2 R708Q). Given our phylogenetic analysis demonstrating this variant's enrichment in approximately 65% of hypoxia-adapted mammals (Table S10 and Figure S5), we systematically evaluated its potential adaptive role through controlled hypoxia exposure experiments. Following 1 month of chronic hypoxia exposure (10% O<sub>2</sub>), transgenic mice exhibited significantly elevated blood oxygen saturation compared to wild-type mice (*M. musculus*) controls (*T*-test,  $P < 1E-4$ ; Fig. 2a; Table S15). Extending these findings to a natural hibernator, we subjected dormice (*G. kelleni*) to identical hypoxic conditions. Both transgenic mice and dormice demonstrated superior oxygen saturation levels relative to wild-type mice, recapitulating the hypoxia-tolerant phenotype observed in natural hibernators. Physiological analyses revealed this adaptive advantage likely stems from enhanced oxygen-carrying capacity, mediated through increased mean red blood cell volume (MCV) of erythrocytes (Fig. 2a; Tables S16 and S17). These results collectively suggest the POMT2 R708Q substitution contributes to hypoxia adaptation.

To further characterize the hypoxia-resistant phenotype, we performed quantitative histopathological analysis using the hypoxia-specific marker pimonidazole. Following 1 month of hypoxic exposure (10% O<sub>2</sub>), comparative tissue staining revealed significantly reduced pimonidazole-positive hypoxic areas in transgenic mice compared to wild-type mice (Fig. 2b; Figures S9 and S10). This finding demonstrates enhanced tissue oxygenation in transgenic mice, providing direct histological evidence for improved hypoxia tolerance at the cellular level (Fig. 2b; Figures S9 and S10).

To investigate hypoxia-induced transcriptional changes associated with the POMT2 R708Q variant, we performed comparative RNA-seq analysis of multiple tissues (heart, liver, spleen, lung, kidney, and muscle) from transgenic and wild-type mice following 1 month of hypoxic exposure. The heart, demonstrating particular transcriptional responsiveness to hypoxia, exhibited 57 differentially expressed genes (DEGs) in mutant mice. Functional enrichment analysis revealed these DEGs were significantly associated with "oxygen carrier activity," "heme binding," and "erythrocyte homeostasis" (Fig. 2c, Tables S18 and S19), indicating substantial remodeling of oxygen transport physiology in transgenic animals. Notably, the observed improvement in blood oxygen saturation (Fig. 2a) correlated with differential expression of BPGM (Fig. 2d), which encodes a key enzyme regulating hemoglobin-oxygen affinity through synthesis of the allosteric effector 2,3-bisphosphoglycerate (2,3-BPG) (Benesch R Fau—Benesch and Benesch 1968). Wild-type mice displayed characteristic hypoxic stress responses including decreased oxygen saturation (Fig. 2a), compensatory erythrocytosis, and dysregulated hemoglobin-related gene expression (Fig. 2d). In contrast, transgenic mice maintained stable hematological parameters without exhibiting these stress responses, demonstrating superior hypoxia adaptation through both physiological and molecular mechanisms.

To elucidate the molecular mechanism underlying the R708Q substitution's functional impact, we generated a protein-protein interaction network from the cardiac DEGs in transgenic mice under hypoxic conditions. Notably, network analysis revealed that 30 of the 57 cardiac DEGs formed a cohesive interaction cluster functionally linked to POMT2 (Fig. 2e). As a protein O-mannosyltransferase, POMT2 catalyzes the critical O-mannosylation of  $\alpha$ -dystroglycan (DAG1) (Willer et al. 2002), with its dysfunction known to cause Walker-Warburg syndrome, a severe congenital muscular dystrophy (Dobyns et al. 1989; Godfrey et al. 2007). The dystrophin-glycoprotein complex (DGC), which includes  $\alpha/\beta$ -dystroglycans, syntrophins, and the central structural protein dystrophin (DMD) (Gao and McNally 2015), plays essential roles in maintaining muscle membrane stability, particularly in cardiac and skeletal muscles (Wilson et al. 2022). Based on this network of DEGs, we propose that POMT2 is involved in adaptation to hypoxia by initially regulating  $\alpha$ -DG and DGC, which interact with other genes involved in the hypoxia response (Fig. 2e).

## *Graphiurus kelleni* exhibits the physiological characteristics of hibernation and the adaptability to hypoxia

The dormouse (*G. kelleni*) investigated in this study demonstrates remarkable physiological adaptations for both hibernation and

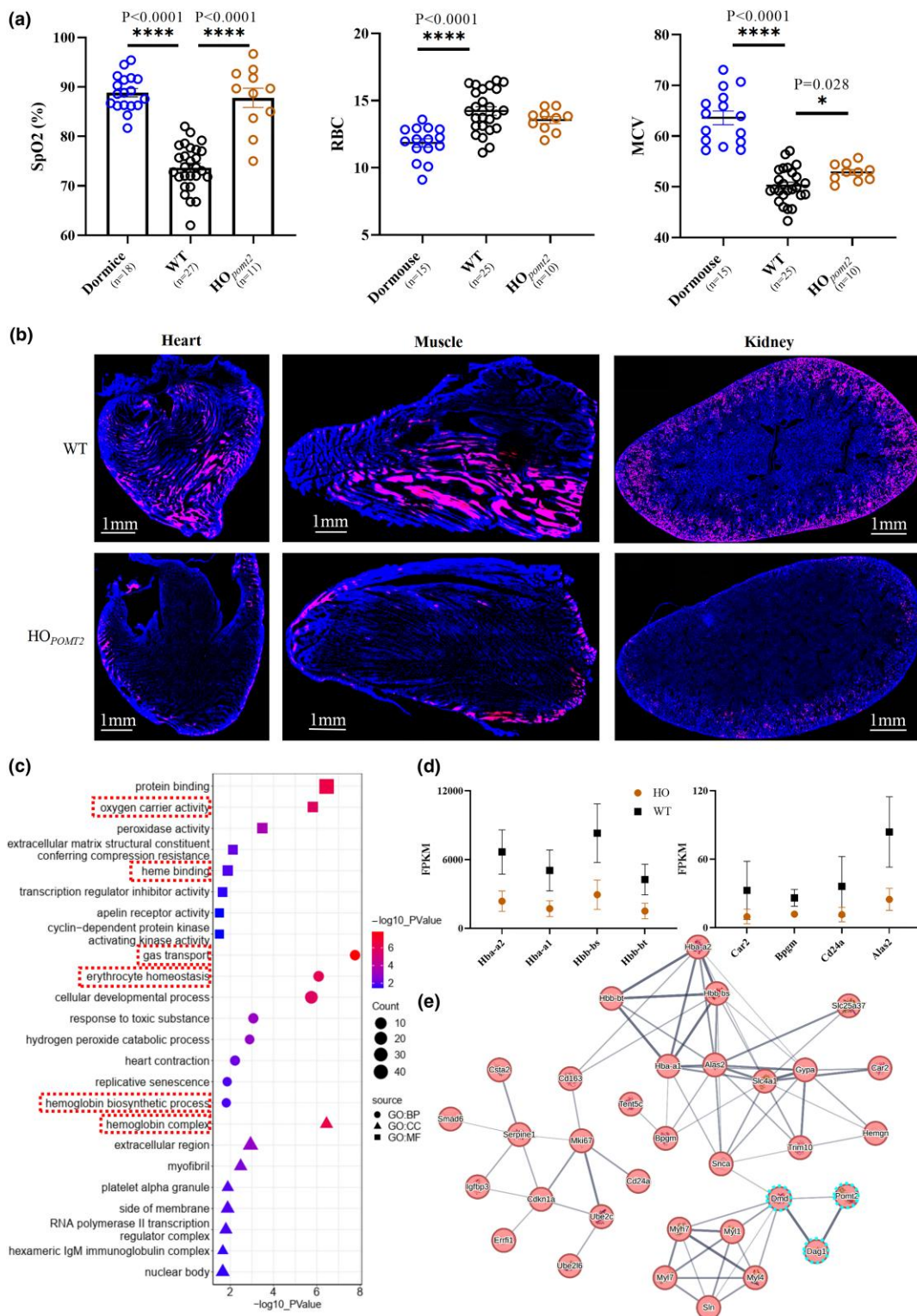


**Figure 2** Hypoxic adaptive phenotype and transcriptional changes in transgenic mice (HO<sub>POMT2</sub>) carrying the homozygous R708Q replacement of POMT2. a) Blood oxygen saturation and routine analysis of blood in dormice (*G. kelleni*), wild-type mice (WT, *M. musculus*), and transgenic mice (HO<sub>POMT2</sub>, *M. musculus* carrying POMT2 R708Q) after 1 month in a hypoxic chamber with 10% oxygen concentration. SpO<sub>2</sub>, blood oxygen saturation; RBC, red blood cells; MCV, mean red blood cell volume. The transgenic mice showed a significant increase in SpO<sub>2</sub> as compared to mice (*T*-test,  $P < 1E-4$ ). b) Pimonidazole staining in different tissues (heart, muscle, and kidney) after prolonged hypoxic exposure (10% O<sub>2</sub>, 4 weeks) of mice and transgenic mice, respectively. c) Enrichment pathway of cardiac DEGs comparing transgenic mice with mice after prolonged hypoxic exposure (10% O<sub>2</sub>, 4 weeks). d) FPKM values of differentially regulated genes (*Hba*, *Hbb*, *Bpgm*, *Alas2*, etc.) associated with hemoglobin and blood oxygen saturation. e) Protein-protein interaction network (Szklarczyk et al. 2023) of 30 of the 57 DEGs which are targeted by POMT2 between transgenic mice and mice after prolonged hypoxic exposure (10% O<sub>2</sub>, 4 weeks). Genes with dashed circles are non-DEGs that have been reported to interact directly with POMT2.

hypoxia tolerance. Although this species lacks the POMT2 R708Q substitution identified as our candidate convergent site, it exhibits exceptional hypoxic tolerance, representing a compelling case of phenotypic convergence. Particularly in functional studies of POMT2 (R708Q) transgenic mice, this species proved invaluable comparative model as a positive control for evaluating hypoxia adaptation phenotypes in natural hibernators.

To characterize torpor physiology in dormice, we conducted continuous body temperature monitoring using implanted telemetry sensors during experimentally induced torpor. Torpor was reliably elicited by maintaining animals at 5 °C in dark conditions with food and water restriction. Throughout the induction period, dormice exhibited characteristic heterothermic responses, demonstrating progressive thermoregulatory adjustments culminating in torpor onset, with body temperature ultimately equilibrating to ambient levels (Fig. 3a). Complementary metabolic measurements using the Sable Promethion system revealed temperature-dependent (30 °C, 18 °C, and 5 °C) oxygen consumption patterns, showing a significant reduction in metabolic rate at 5 °C (Fig. 3b; Figure S11 and Table S20). This metabolic suppression phenotype parallels observations in other heterothermic species such as tenrecs (Treat et al. 2018), confirming the dormouse's capacity for profound metabolic depression during torpor. In contrast to the heterothermic dormice (*G. kelleni*), homeothermic mice (*M. musculus*) exhibited fundamentally different metabolic responses to cold exposure, increasing their oxygen consumption to maintain stable body temperatures (Fig. 3b; Table S20). The dormice's torpor state, characterized by reduced body temperature and suppressed energy metabolism, suggested corresponding decreases in tissue oxygen demand. Physiological measurements confirmed this hypothesis, revealing significantly decreased blood oxygen saturation during torpor ( $P < 1E-4$ ; Fig. 3c; Table S21). To further quantify tissue-specific hypoxia, we performed pimonidazole staining on muscle, liver, and kidney samples comparing torpid versus active states. Histological analysis demonstrated substantially expanded hypoxic areas in all examined tissues during torpor (Fig. 3d and e; Figure S12 and Table S22), providing direct histological evidence of systemic hypoxia during metabolic suppression. These findings collectively establish that torpor in dormice creates a pronounced hypoxic microenvironment at both circulatory and tissue levels.

To investigate molecular adaptations to hypoxia during torpor, we performed comparative transcriptomic analysis of multiple dormouse tissues (liver, spleen, lung, kidney, heart, and muscle) between torpid and active states. Functional enrichment analysis of DEGs revealed significant involvement in hypoxia-related pathways, including “response to hypoxia,” “response to decreased oxygen levels,” and “response to oxygen levels” (Figures S13 to S15 and Table S23). Notably, we observed up-regulation of *HMOX2* during torpor (Figure S13), encoding heme oxygenase-2 which modulates hemoglobin metabolism. This finding aligns with previous reports that elevated *HMOX2* expression enhances heme catabolism, potentially facilitating hemoglobin homeostasis under hypoxic conditions (Yang et al. 2016). Conversely, several hypoxia-responsive genes including *DDIT4*, *CXCL12*, *CXCR4*, *NOS2*, and *ANGPTL4* showed marked down-regulation during torpor (Figure S13). While these expression patterns suggest potential modulation of hypoxia signaling pathways during metabolic suppression of hibernation, the

functional consequences of these transcriptional changes require further experimental validation.

## Discussion

### A convergent amino acid substitution of POMT2 in hibernating mammals showed evidence of involvement in hypoxia adaptation

Through comprehensive comparative genomic analysis of six hibernating and six non-hibernating mammalian species, we identified 5,561 high-confidence one-to-one orthologous protein-coding genes. Based on the CCS method (Xu et al. 2017) and the MEME method implemented in HyPhy (Murrell et al. 2012), we systematically screened for molecular signatures of convergent evolution and positive selection among hibernators. Remarkably, phylogenetic analysis across 244 mammalian species revealed that the POMT2 R708Q substitution showed the highest prevalence among hypoxia-adapted species, strongly suggesting its functional importance in hypoxia adaptation mechanisms. This finding established POMT2 R708Q as our primary candidate for subsequent functional validation. Phylogenetic analysis employing the methods of PCOC (Rey et al. 2018) and HeIST (Hibbins et al. 2020) suggested hemiplasy as an alternative interpretation.

Functional validation of the POMT2 R708Q variant in transgenic mice demonstrated significant hypoxia resistance compared to wild-type controls. Following chronic hypoxic exposure (10% O<sub>2</sub> for 1 month), transgenic mice maintained superior blood oxygen saturation as compared to wild-type mice (~90% vs. ~70% SpO<sub>2</sub>). Histopathological analysis using pimonidazole staining confirmed enhanced tissue oxygenation in transgenic mice, with significantly reduced hypoxic areas across multiple organs. Transcriptomic profiling revealed coordinated up-regulation of oxygen transport pathways, particularly genes annotated with “oxygen carrier activity,” providing molecular correlates for the observed physiological adaptation. All of these lines of evidence, from whole-organism physiology to cellular responses and gene expression regulation, establish POMT2 as a key mediator of hypoxia adaptation in hibernating mammals.

### The hibernation phenotype of *G. kelleni* was revealed for the first time

Hibernation represents a conserved survival strategy that enables animals to endure extreme environmental challenges, including low temperatures and resource scarcity. During this physiological state, hibernators exhibit profound metabolic suppression characterized by significantly reduced body temperature, cardiovascular activity, and respiratory rate, all contributing to markedly decreased oxygen consumption. Our experimental induction of torpor in *G. kelleni* recapitulated these classic hibernation phenotypes, demonstrating a dramatic decline in both metabolic rate (VO<sub>2</sub>) and core body temperature. Physiological measurements revealed corresponding reductions in blood oxygen saturation to approximately 70% SpO<sub>2</sub> during

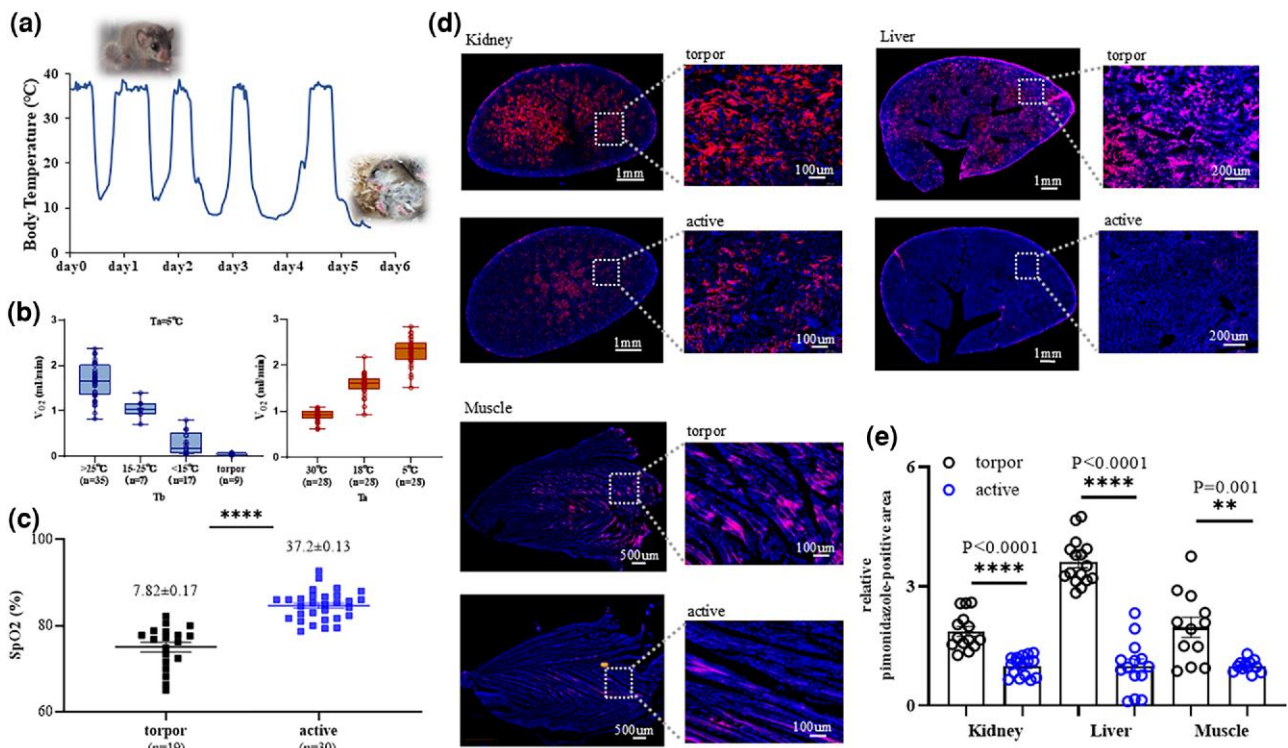


**Figure 3** Physiological changes in the dormouse after artificial induction of torpor. a) Body temperature ( $T_b$ ) of dormouse during the process of torpor recorded by real-time telemetry temperature loggers (a single representative animal exposed to an ambient temperature ( $T_a$ ) of  $5^\circ\text{C}$  for multiple days with food deprivation). b) Left panel: oxygen consumption of dormice at variable body temperature when exposed to an ambient temperature ( $T_a$ ) of  $5^\circ\text{C}$  with food deprivation, and right panel: oxygen consumption of mice exposed to different  $T_a$  of  $30^\circ\text{C}$ ,  $18^\circ\text{C}$ , and  $5^\circ\text{C}$  with food. c) Blood oxygen saturation (SpO<sub>2</sub>) of dormice under torpor and active state; numbers associated with the boxes represents rectal temperature ( $^\circ\text{C}$ ; means  $\pm$  SEM). d) Pimonidazole staining of tissues (kidney, liver, and muscle) from dormice under torpor and active state. e) Quantitative analysis of pimonidazole-positive cells in the low-oxygen state in d) using  $T$ -test; pimonidazole-positive cells in the active state were normalized to 1. Data are shown as means  $\pm$  SEM.

torpor. Complementary histochemical analysis using pimonidazole staining provided direct visual evidence of tissue-level hypoxia during metabolic suppression. Transcriptomic profiling further identified coordinated regulation of hypoxia-responsive pathways during torpor, revealing molecular adaptations to oxygen limitation. Collectively, *G. kelleni* exhibit both the characteristic physiological signatures of hibernation and robust adaptive responses to hypoxic stress.

Overall, our study characterizes the hypoxia adaptation phenotype in hibernating mammals and elucidates key genetic components underlying this physiological adaptation. While our findings provide substantial mechanistic insights, the complexity of hibernation biology need for further investigation of additional molecular mechanisms that contribute to hibernation phenotypes beyond those identified in our current work.

## Materials and methods

### Genome assembly

In total, 253.3 Gb and 200.1 Gb raw reads of *G. kelleni* and *N. procyonoides* were generated, respectively. For de novo genome assembly, we used the PromethION long-read sequencing technologies (Oxford Nanopore Technologies [ONT]) with NextDenovo (<https://github.com/Nextomics/NextDenovo>). Because of the

high error rate of the ONT raw reads, the original subreads were first self-corrected using NextCorrect, thereby generating consistent sequences (CNS reads). Comparison of CNS was then performed with the NextGraph module to capture correlations of CNS. Based on the CNS correlations, the draft genome was assembled. For genome of *G. kelleni*, using the error correction parameters: read\_cutoff 2k; seed\_cutoff 30k, and the assemble parameters: nextgraph -a 1 -n 49 -Q 6 -l 0.48 -S 0.24 -N 2 -r 0.25 -m 1.86 -C 456964 -z 11. For genome of *N. procyonoides*, using the error correction parameters: read\_cutoff 2k; seed\_cutoff 25k, and the assemble parameters: nextgraph -a 1 -n 45 -Q 5 -l 0.22 -S 0.70 -N 1 -r 0.13 -m 4.00 -C 1257840 -z 20. To improve the accuracy of the assemblies, the contigs were refined with Racon using ONT long reads and Nextpolish using Illumina short reads with default parameters. To discard possibly redundant contigs and to generate a final assembly, similarity searches were performed with the parameters “identity 0.8 –overlap 0.8.” Finally, we obtained the final genome sequence of *G. kelleni* with a genome size of 2.7 Gb, a contig N50 size of 26.6 Mb, and contig number equal to 1,943. For *N. procyonoides*, the genome size was found to be 2.6 Gb, with the contig N50 size being 51.5 Mb and the contig number 1,381. The completeness of genome assembly was assessed using BUSCO v3.0.1 (Simão et al. 2015) (Benchmarking Universal Single Copy Orthologs). To evaluate the accuracy of the assembly, all the Illumina paired end reads were mapped to the assembled genome using BWA (Burrows–Wheeler Aligner).

Both the mapping rate and the genome coverage of sequencing reads were assessed using SAMtools v0.1.1855 while the base accuracy of the assembly was calculated with bcftools.

## Genome annotation

For repeat annotation, we first annotated the tandem repeats using the software MISA (Thiel et al. 2003) and identified 22,596,818 and 21,790,806 simple repeat sequences (SSRs) in the *G. kelleni* and *N. procyonoides* genomes, respectively. An ab initio repeat library was first predicted using MITE-hunter and RepeatModeler with default parameters when performing the transposable element (TE) identification. The library obtained was then aligned to TEclass Repbase (<http://www.girinst.org/rebase>) to classify the type of each repeat family. For further identification of the repeats throughout the genome, RepeatMasker was applied to search for known and novel TEs by mapping sequences against the de novo repeat library and Repbase TE library. The results showed that the dormouse and raccoon dog genomes contained 42.80% and 33.33% repeated sequences, respectively (Figure S4 and Tables S24 and S25). Gene prediction of the two de novo genomes were annotated by CESAR (Sharma and Hiller 2019). For the dormouse, we used mouse protein-coding genes as the reference set; CESAR annotated 18,415 protein-coding genes (a total of 178,744 protein-coding exons). For the raccoon dog, we used human protein-coding genes as the reference set; CESAR annotated 17,544 genes (a total of 178,703 protein-coding exons). We used the longest isoform from each of these genes for exon annotation in the two species.

## Comparative genomics and positive selection analysis

Across 12 mammalian species (*M. musculus*, *H. sapiens*, *F. catus*, *P. alecto*, *S. araneus*, *G. kelleni*, *N. coucang*, *N. procyonoides*, *U. americanus*, *H. armiger*, *E. europaeus*, and *D. novemcinctus*), the one-to-one orthologous genes were identified by OthoFinder v2.5.5 with parameters `-M msa -s tree`. The putative orthologs were aligned using PRANK (Löytynoja and Goldman 2008) with parameters `prank -f=fasta -F -codon -noxml -notree -nopost`. After the alignment and trimming processes, we finally obtained a total of 5,561 high-confidence one-to-one orthologous protein-coding genes. Based on a method for detecting convergence at conservative Sites (CCS) (Xu et al. 2017), we established a phylogenetic framework comprising six hibernating mammals as the foreground convergent clade, five non-hibernating mammals as background lineages, with *D. novemcinctus* as the outgroup. Convergence was strictly defined at conserved sites meeting two criteria: (i) all background species or all foreground species maintained the ancestral state (as determined by the outgroup) and (ii) at least four hibernating species (more than half of the hibernators) shared identical derived mutations. In addition, the program MEME in HyPhy software v2.5.71 was implemented to detect sites under episodic positive selection in hibernating lineages (parameters: `hyphy meme -alignment cds.aln -tree hyphy.tree -branches Foreground -output MEME.json`). This approach applies a maximum likelihood methodology and uses a likelihood ratio test for positive selection on each site, comparing modes which allow or disallow positive

diversifying selection at a subset of branches ( $dN/dS > 1$ ). In this method, the neutral null hypothesis is considered to represent the worst-case scenario for the inference, and the obtained nominal *P*-value serves as the upper bound of the true *P*-value. Consequently, the nominal *P*-value is used as the final *P*-value in this approach (Murrell et al. 2012). BUSTED was used as a complementary test for gene-wide selection at the gene level within pre-specified lineages (parameters: `hyphy BUSTED -srv Yes -alignment cds.aln -tree tree -branches hibernating-species`). The Bonferroni correction for multiple comparisons sets the threshold for statistical significance at  $P < 0.05$ , with all *P*-values being adjusted accordingly. The PCOC method (Rey et al. 2018) was used to identify the a posteriori probability of convergent shift substitutions occurring on branches where the hypoxia phenotype changed.

## Estimating the probability of hemiplasy, homoplasy, and their combination

The signals of incomplete lineage sorting and convergent evolution may potentially be confused with each other. To estimate the contribution of convergent evolution (homoplasy) and/or incomplete lineage sorting (hemiplasy) to the origin of the R to Q POMT2 substitution, we estimated the relative probabilities of hemiplasy, homoplasy, and their combination within our phylogenetic framework using HeISt (Hibbins et al. 2020). Initially, we calculated genome-wide gene concordance factors, defined as the percentage of gene trees containing a given branch found in the species tree. We calculated gene tree concordance factors using the species tree (Fig. 1b) and gene trees inferred from 16,579 filtered amino acid sequence alignments (see above) using IQ-TREE v.1.6.12 (Nguyen et al. 2015) with the parameters `-m LG+G4 -nt 1000`. Subsequently, because the large number of species (up to 230) in our phylogenetic framework exceeded our computing resources and the processing capabilities of HeISt, we opted to reduce the size of the dataset investigated. For our analysis, we performed simulations on a total of 1,500 datasets, which were categorized into three groups based on the number of randomly selected species from our phylogenetic tree (i.e. 20, 25, and 30). However, the simulations with 25 and 30 species had a low yield of valid outputs (<50%) that included the focal loci (Figure S8 and Table S13). Consequently, we focused on simulations with datasets of 20 randomly selected species, which provided a sufficient number of valid simulations. A total of 1,000 randomized datasets (each including 20 species) were generated by randomly pooling species from our phylogenetic framework. The phylogenetic trees with gene concordance factors of these species in randomized datasets were generated using `nw_prune` script in `newick_utils` tools (Junier and Zdobnov 2010) with species tree (Fig. 1b) as the reference. Finally, HeISt was executed on each randomized dataset with the parameters `-s 0.005 -n 108`. Additionally, an introgression event was modeled between two randomly selected species, using the parameters `probability = 10-5` and `timing = 0.3`. The Fitch parsimony method in HeISt was employed to infer the number of amino acid substitutions required to account for the trait pattern in each random dataset. HeISt uses `ms` (Hudson 2002) to simulate gene trees from a specified species tree and, subsequently, simulates the evolution of a nucleotide along each of these simulated gene

trees using *Seq-gen* (Rambaut and Grassly 1997). Simulated loci with transformed nucleotide states (0/1 for ancestral or derived mutations, respectively) that match the character traits on the species tree (in this case, Q or R) were considered to be focal loci and only focal loci reflecting the specific character states in the species tree were considered. The predominant biological cause (hemiplasy, homoplasy, and combination) with the most focal loci was considered to be the origin of amino acid substitutions leading to the observed character states for that particular randomized dataset. Datasets in which no focal locus was identified were excluded from the analysis.

## Construction of POMT2 point mutant mice

A C57BL/6 *M. musculus* model with a p.R708Q, c.2123 G>A mutation at the murine *POMT2* locus (reference sequence, ENSMUSG00000034126) was constructed by CRISPR/Cas-mediated genome engineering (Shanghai Biomodel Organism Science & Technology Development Co., Ltd). Briefly, Cas9 mRNA, gRNA, and donor DNA were micro-injected into the fertilized eggs of C57BL/6J *M. musculus* to obtain F0 generation mice with the required mutation at the target site. The F0 generation mice were then mated with C57BL/6J *M. musculus* to obtain homozygous mutation-positive F1 generation mice.

## Exposure of transgenic mice and mice to prolonged hypoxia

Eight-week-old transgenic mice and wild-type mice were weighed and placed in a polycarbonate hypoxic chamber (Coy Laboratory Products) at 10% oxygen concentration. The oxygen level in the chamber was controlled automatically by balancing the air with N<sub>2</sub>. After prolonged hypoxic exposure for four weeks, we monitored the blood oxygen saturation (SpO<sub>2</sub>) continuously (MP150, BIOPAC Systems). Arterial blood was taken for routine blood analysis, and RNA tissue samples were frozen in liquid nitrogen for transcriptome sequencing. The degree of right ventricular hypertrophy was determined by the weight ratio of the right ventricle to the heart; the weight of the spleen was also recorded.

## Artificially induced dormouse into torpor and phenotypic detection

We implanted dormice with real-time telemetry temperature loggers (DST nanoRF-T; Star-Oddi) to monitor their body temperature continuously and induced a state of torpor by housing the animals in a darkroom at 5 °C without food and water. To monitor the oxygen consumption rate of the dormice, we placed them in a Metabolism and Behavior Monitoring system (Sable Systems International, Promethion). Male dormice weighing between 25 and 35 g were placed in the metabolic cage with flow rate of air 2,000 mL/min, at 30 °C for 3 days, 18 °C for 3 days, 5 °C for 5 days under conditions of fasting for solids and liquids. During this period, we measured the dormouse rectal temperature one or twice a day, and the average oxygen consumption was calculated. The BioPAC MP-150 Data Acquisition System was used to record SpO<sub>2</sub> values.

## Immunofluorescence staining

To ascertain the hypoxia status of mouse and dormouse tissues, solid pimonidazole HCl [HPI, HP8-100 Kit] was administered by abdominal injection at a concentration of 60 mg/kg 2 h before tissue collection in mice and active dormice and 18 h before tissue collection in torpor dormice (taking into consideration that the oxygen consumption rate slows down during hibernation or torpor). The hypoxia status of the tissue was determined by means of solid pimonidazole HCl incorporation. Hypoxyprobe RedAPC Kit is a hypoxia probe labeling kit developed by HPI, Inc. and based on hypoxia probe antibody technology. It is a technique for measuring cellular hypoxia at the cellular level by utilizing the selective binding ability of reducing nitro groups to hypoxic cells. Pimonidazole is a novel hypoxic cell marker, and HPI, Inc. has nitroimidazole-specific antibodies that can be used for immunohistochemical, enzyme-linked immunosorbent assay, and flow cytometry detection. Hypoxyprobe is highly water soluble and chemically stable and is taken up very efficiently by tissues *in vivo*. (For the detailed content and references, please see <http://www.hypoxyprobe.com/knowledge-center.html>.) For immunofluorescence, the mice were perfused with phosphate buffered saline by cardiac perfusion techniques, and 4% paraformaldehyde (PFA) was used for tissue fixation. To fix the sample, kidney, liver, and muscle tissue was treated with 4% PFA overnight at 4 °C followed by dehydration by 25% sucrose, then replaced with 30% sucrose twice. 20 μm thick sections were obtained using cryostat sectioning. The following reagents were used for immunostaining: Hypoxyprobe RedAPC Kit (HP8-100 kit, 5914) of concentration 1:200, DAPI (Beyotime, P0131). Images were taken with a TissueFAXs cell analysis system (TissueGnostics GmbH, Austria).

## Transcriptome analysis

Tissues for RNA sequencing were frozen with liquid nitrogen immediately after euthanasia. After RNA extraction, RNA integrity was assessed using the Fragment Analyzer 5400 (Agilent Technologies, CA, United States). Total RNA was used as input material for the RNA sample preparations. Sequencing libraries were generated using the NEBNext® Ultra™ RNA Library Prep Kit from Illumina® (NEB, United States) following the manufacturer's recommendations, and index codes were added to allow attribution of sequences to each sample. After cluster generation of the index-coded samples, the library preparations were sequenced on an Illumina Novaseq 6000 platform and 150 bp paired-end reads were generated. We used Fastp (v0.19.7) (Chen et al. 2018) to discard paired reads if either one read contained adapter contamination, or more than 10% of bases were uncertain in either one read, and paired reads if the proportion of low quality (Phred quality <5) bases was over 50% in either one of the reads. After these quality controls, we obtained clean reads for bioinformatics analysis. Before alignment, reads were trimmed based on their quality scores using the quality trimming program (-a 25), Btrim (Kong 2011). Reads were aligned to our reference genomes of mouse (GRCm39) and dormouse using TopHat (v2.1.1) (Trapnell et al. 2009) and then assembled using Cufflinks (v2.2.1 with -G parameter). Differential expression of genes in the different tissues was calculated using Cuffdiff

(Trapnell et al. 2012). Gene Ontology enrichment analyses were performed using g: profiler (<https://biit.cs.ut.ee/gprofiler/>).

## Acknowledgments

This work was supported by the Animal Branch of the Germplasm Bank of Wild Species, Chinese Academy of Sciences (Large Research Infrastructure Funding). We would like to thank the Institutional Center for Shared Technologies and Facilities of the Kunming Institute of Zoology (KIZ), Chinese Academy of Sciences (CAS), for providing us with confocal microscopy image acquisition/flow cytometric analysis, and we are grateful to Cong Li for his technical support. We thank the staff members of the National Research Facility for Phenotypic & Genetic Analysis of Model Animals (Primate Facility) (<https://cstr.cn/31137.02.NPRC>) for providing technical support and assistance in data collection and analysis.

## Author contributions

L.Z. led the project and designed the study. L.Z., D.-D.W., J.Z., and X.Z. prepared the manuscript. L.Z., J.Z., X.Z., N.L., J.H., F.H., H.D., M.H., and V.S. performed the data analysis. L.Z., J.Z., and X.Y. performed some sampling and experiments. All authors edited and approved the manuscript.

## Supplementary material

Supplementary material is available at *Molecular Biology and Evolution* online.

## Funding

This work was supported by the National Natural Science Foundation of China (32170513, 31801053, 32400351), the Young Academic and Technology Leaders Project of Yunnan Province (202205AC160068), Yunnan Fundamental Research Projects (202501AW070021, 202401CF070063), and Yunnan Province (202305AH340006).

## Ethical approval and consent to participate

All animal care and experimental procedures were conducted in compliance with the guidelines of the Animal Care and Use Committee (IACU) of the Kunming Institute of Zoology, Chinese Academy of Sciences (approval number: IACUC-RE-2023-09-006, IACUC-RE-2023-12-006).

## Conflicts of interest

The authors declare no conflict of interest.

## Data availability

The DNA sequences reported in this study have been deposited in the Genome Sequence Archive database under accession ID CRA016523 (<https://bigd.big.ac.cn/gsa/browse/CRA016523>).

## References

- Azevedo L, Serrano C, Amorim A, Cooper DN. Trans-species polymorphism in humans and the great apes is generally maintained by balancing selection that modulates the host immune response. *Hum Genomics*. 2015;9:21. <https://doi.org/10.1186/s40246-015-0043-1>.
- Bai L et al. Hypoxic and cold adaptation insights from the Himalayan Marmot genome. *iScience*. 2019;11:519–530. <https://doi.org/10.1016/j.isci.2018.11.034>.
- Benesch R, Benesch RE. Oxygenation and ion transport in red cells. *Science*. 1968;160:83. <https://doi.org/10.1126/science.160.3823.83.a>.
- Biggar KK et al. Modulation of gene expression in key survival pathways during daily Torpor in the gray mouse Lemur, *Microcebus murinus*. *Genomics Proteomics Bioinformatics*. 2015;13:111–118. <https://doi.org/10.1016/j.gpb.2015.03.001>.
- Chen S, Zhou Y, Chen Y, Gu J. Fastp: an ultra-fast all-in-one FASTQ preprocessor. *Bioinformatics*. 2018;34:i884–i890. <https://doi.org/10.1093/bioinformatics/bty560>.
- Dobyns WB et al. Diagnostic criteria for Walker-Warburg syndrome. *Am J Med Genet*. 1989;32:195–210. <https://doi.org/10.1002/ajmg.1320320213>.
- Footo AD et al. Convergent evolution of the genomes of marine mammals. *Nat Genet*. 2015;47:272–275. <https://doi.org/10.1038/ng.3198>.
- Gao QQ, McNally EM. The dystrophin complex: structure, function, and implications for therapy. *Compr Physiol*. 2015;5:1223–1239. <https://doi.org/10.1002/j.2040-4603.2015.tb00638.x>.
- Geiser F. Hibernation. *Curr Biol*. 2013;23:R188–R193. <https://doi.org/10.1016/j.cub.2013.01.062>.
- Godfrey C et al. Refining genotype phenotype correlations in muscular dystrophies with defective glycosylation of dystroglycan. *Brain*. 2007;130:2725–2735. <https://doi.org/10.1093/brain/awm212>.
- Hibbins MA-O, Gibson MA-O, Hahn MA-O. Determining the probability of hemiplasy in the presence of incomplete lineage sorting and introgression. *Elife*. 2020;21:e63753. <https://doi.org/10.7554/eLife.63753>.
- Hudson RR. Generating samples under a Wright-Fisher neutral model of genetic variation. *Bioinformatics*. 2002;8:337–338. <https://doi.org/10.1093/bioinformatics/18.2.337>.
- Junier T, Zdobnov EM. The Newick utilities: high-throughput phylogenetic tree processing in the UNIX shell. *Bioinformatics*. 2010;26:1669–1670. <https://doi.org/10.1093/bioinformatics/btq243>.
- Kong Y. Btrim: a fast, lightweight adapter and quality trimming program for next-generation sequencing technologies. *Genomics*. 2011;98:152–153. <https://doi.org/10.1016/j.ygeno.2011.05.009>.
- Lee PA-O, Chandel NA, Simon MA. Cellular adaptation to hypoxia through hypoxia inducible factors and beyond. *Nat Rev Mol Cell Biol*. 2020;21:268–283. <https://doi.org/10.1038/s41580-020-0227-y>.
- Löytynoja A, Goldman N. Phylogeny-aware gap placement prevents errors in sequence alignment and evolutionary analysis. *Science*. 2008;320:1632–5885. <https://doi.org/10.1126/science.1158395>.
- Matos-Cruz V et al. Molecular prerequisites for diminished cold sensitivity in ground squirrels and hamsters. *Cell Rep*.

- 2017:21:3329–3337. <https://doi.org/10.1016/j.celrep.2017.11.083>.
- Murrell B *et al.* Detecting individual sites subject to episodic diversifying selection. *PLoS Genet.* 2012;8:e1002764. <https://doi.org/10.1371/journal.pgen.1002764>.
- Nguyen LT, Schmidt HA, von Haeseler A, Minh BQ. IQ-TREE: a fast and effective stochastic algorithm for estimating maximum-likelihood phylogenies. *Mol Biol Evol.* 2015;32:268–274. <https://doi.org/10.1093/molbev/msu300>.
- Ou J *et al.* iPSCs from a hibernator provide a platform for studying cold adaptation and its potential medical applications. *Cell.* 2018;173:851–863.e116. <https://doi.org/10.1016/j.cell.2018.03.010>.
- Rambaut A, Grassly NC. Seq-Gen: an application for the Monte Carlo simulation of DNA sequence evolution along phylogenetic trees. *Comput Appl Biosci.* 1997;13:235–238. <https://doi.org/10.1093/bioinformatics/13.3.235>.
- Rey C, Guéguen L, Sémon M, Boussau B. Accurate detection of convergent amino-acid evolution with PCOC. *Mol Biol Evol.* 2018;35:2296–2306. <https://doi.org/10.1093/molbev/msy114>.
- Sharma V, Hiller M. Coding exon-structure aware realigner (CESAR): utilizing genome alignments for comparative gene annotation. *Methods Mol Biol.* 2019;1962:179–191. [https://doi.org/10.1007/978-1-4939-9173-0\\_10](https://doi.org/10.1007/978-1-4939-9173-0_10).
- Simão FA, Waterhouse RM, Ioannidis P, Kriventseva EV, Zdobnov EM. BUSCO: assessing genome assembly and annotation completeness with single-copy orthologs. *Bioinformatics.* 2015;31(19):3210–2. <https://doi.org/10.1093/bioinformatics/btv351>.
- Szklarczyk D *et al.* The STRING database in 2023: protein-protein association networks and functional enrichment analyses for any sequenced genome of interest. *Nucleic Acids Res.* 2023;51:D638–D646. <https://doi.org/10.1093/nar/gkac1000>.
- Thiel T, Michalek W, Varshney R, Graner A. Exploiting EST databases for the development and characterization of gene-derived SSR-markers in barley (*Hordeum vulgare* L.). *Theor Appl Genet.* 2003;106:411–122. <https://doi.org/10.1007/s00122-002-1031-0>.
- Thienel MA *et al.* Immobility-associated thromboprotection is conserved across mammalian species from bear to human. *Science.* 2023;380:6178–6187. <https://doi.org/10.1126/science.abo5044>.
- Trapnell C *et al.* Differential gene and transcript expression analysis of RNA-seq experiments with TopHat and Cufflinks. *Nat Protoc.* 2012;7:562–578. <https://doi.org/10.1038/nprot.2012.016>.
- Trapnell C, Pachter L, Salzberg SL. TopHat: discovering splice junctions with RNA-Seq. *Bioinformatics.* 2009;25:1105–1111. <https://doi.org/10.1093/bioinformatics/btp120>.
- Treat MA *et al.* Extreme physiological plasticity in a hibernating basoendothermic mammal, *Tenrec ecaudatus*. *J Exp Biol.* 2018;221:jeb185900. <https://doi.org/10.1242/jeb.185900>
- Willer T, Amselgruber W, Deutzmann R, Strahl S. Characterization of POMT2, a novel member of the PMT protein O-mannosyltransferase family specifically localized to the acrosome of mammalian spermatids. *Glycobiology.* 2002;12:771–783. <https://doi.org/10.1093/glycob/cwf086>.
- Wilson DGS, Tinker A, Iskratsch TA. The role of the dystrophin glycoprotein complex in muscle cell mechanotransduction. *Commun Biol.* 2022;5:1022. <https://doi.org/10.1038/s42003-022-03980-y>.
- Xu S *et al.* Genome-wide convergence during evolution of mangroves from woody plants. *Mol Biol Evol.* 2017;34:1008–1015. <https://doi.org/10.1093/molbev/msw277>.
- Yang D *et al.* *HMOX2* functions as a modifier gene for high-altitude adaptation in Tibetans. *Hum Mutat.* 2016;37:216–223. <https://doi.org/10.1002/humu.22935>.
- Yang Y *et al.* Integrated transcriptomics and metabolomics reveal protective effects on heart of hibernating Daurian ground squirrels. *J Cell Physiol.* 2023;238:2724–2748. <https://doi.org/10.1002/jcp.31123>.
- Zoonomia Consortium. A comparative genomics multitool for scientific discovery and conservation. *Nature.* 2020;587:240–245. <https://doi.org/10.1038/s41586-020-2876-6>.